



HAL
open science

Amorphous Iron–Manganese Oxyfluorides, Promising Catalysts for Oxygen Evolution Reaction under Acidic Media

Kévin Lemoine, Zahra Gohari-Bajestani, Romain Moury, Alexandre Terry, Amandine Guiet, Jean-Marc Grenèche, Annie Hémon-Ribaud, Nina Heidary, Vincent Maisonneuve, Nikolay Kornienko, et al.

► **To cite this version:**

Kévin Lemoine, Zahra Gohari-Bajestani, Romain Moury, Alexandre Terry, Amandine Guiet, et al.. Amorphous Iron–Manganese Oxyfluorides, Promising Catalysts for Oxygen Evolution Reaction under Acidic Media. ACS Applied Energy Materials, 2021, 4 (2), pp.1173-1181. 10.1021/acsaem.0c02417 . hal-03888230

HAL Id: hal-03888230

<https://hal.science/hal-03888230>

Submitted on 7 Dec 2022

HAL is a multi-disciplinary open access archive for the deposit and dissemination of scientific research documents, whether they are published or not. The documents may come from teaching and research institutions in France or abroad, or from public or private research centers.

L'archive ouverte pluridisciplinaire **HAL**, est destinée au dépôt et à la diffusion de documents scientifiques de niveau recherche, publiés ou non, émanant des établissements d'enseignement et de recherche français ou étrangers, des laboratoires publics ou privés.

This document is confidential and is proprietary to the American Chemical Society and its authors. Do not copy or disclose without written permission. If you have received this item in error, notify the sender and delete all copies.

Amorphous iron-manganese oxyfluorides, promising catalysts for Oxygen Evolution Reaction under acidic media

Journal:	<i>ACS Applied Energy Materials</i>
Manuscript ID	ae-2020-024172
Manuscript Type:	Article
Date Submitted by the Author:	29-Sep-2020
Complete List of Authors:	Lemoine, Kevin; IMMM-UMR 6283 CNRS, LUNAM, Oxydes et Fluorures Gohari-Bajestani, Zahra; IMMM-UMR 6283 CNRS, LUNAM, Oxydes et Fluorures Moury, Romain; Universite du Maine IUT du Mans, Institut des Matériaux et des Molécules du Mans Terry, Alexandre; IMMM-UMR 6283 CNRS, LUNAM, Oxydes et Fluorures Guet, Amandine; Le Mans Université, IMMM-UMR 6283 CNRS, LUNAM, Oxydes et Fluorures Greneche, Jean-Marc; IMMM-UMR 6283 CNRS, LUNAM, Oxydes et Fluorures Hémon-Ribaud, Annie; IMMM-UMR 6283 CNRS, LUNAM, Oxydes et Fluorures Heidary, Nina; Université de Montréal, Department of Chemistry Maisonneuve, Vincent; Faculté des Sciences et Techniques, Institut des Molécules et des Matériaux du Mans - UMR CNRS 6283 Kornienko, Nikolay; University of Montreal, Chemistry Lhoste, Jerome; IMMM-UMR 6283 CNRS, LUNAM, Oxydes et Fluorures

SCHOLARONE™
Manuscripts

1
2
3 **Amorphous iron-manganese oxyfluorides, promising catalysts for**
4
5
6 **Oxygen Evolution Reaction under acidic media**
7

8
9 *Kévin Lemoine,^{1,‡} Zahra Gohari-Bajestani,¹ Romain Moury,¹ Alexandre Terry,¹*

10
11
12 *Amandine Guiet,¹ Jean-Marc Grenèche,¹ Annie Hémon-Ribaud,¹ Nina Heidary,²*

13
14
15
16 *Vincent Maisonneuve,² Nikolay Kornienko,^{2,*} Jérôme Lhoste^{1,*}*
17

18
19
20 ¹Institut des Molécules et Matériaux du Mans (IMMM), UMR 6283 CNRS, Le Mans Université, Avenue
21 Olivier Messiaen, 72085 Le Mans Cedex 9, France

22
23
24 ²Department of Chemistry, Université de Montréal, Roger-Gaudry Building, Montreal, Quebec, H3C
25 3J7, Canada

26
27
28
29
30 ‡Present address: Department of Chemistry, Faculty of Science, Gakushuin University, 1-5-1 Mejiro,
31 Toshima-ku, Tokyo 171-8588, Japan

32
33
34 *corresponding authors: jerome.lhoste@univ-lemans.fr and nikolay.kornienko@umontreal.ca
35

36
37 **Keywords:** amorphous oxyfluorides, acid-stable electrocatalysis, oxygen evolution reaction, renewable
38 energy, heterogeneous catalysis
39
40
41
42
43
44
45
46
47
48
49
50
51
52
53
54
55
56
57
58
59
60

Abstract

The development of earth-abundant catalysts for the oxygen evolution reaction (OER) in acidic media represents a significant challenge in the context of polymer electrolyte membrane (PEM) based electrolysis. In this scope, transition metal oxides constitute an emerging alternative to Ir and Ru oxides. Notably, Mn-oxides are amongst the few that have sufficient stability in acidic electrolytes, but their performance still lacks behind Ir/Ru oxides. To this end, the modification of Mn oxides' structure, crystallinity (or amorphous structure), and/or composition may work to enhance their catalytic activity. In this report, we focused our attention on the development mixed-metal Mn-Fe based catalysts containing highly electronegative fluorine ions as acid-stable OER catalysts. Alongside of previously established $\text{MnFe}_2\text{F}_8(\text{H}_2\text{O})_2$ and $\text{MnFe}_2\text{F}_{5.8}\text{O}_{1.1}$ oxyfluorides, a hydrated fluoride, $\text{MnFeF}_5(\text{H}_2\text{O})_2$, was prepared by microwave-assisted solvothermal synthesis and its subsequent thermal treatment under air yielded the corresponding oxyfluoride $\text{MnFeF}_{4.6}\text{O}_{0.2}$. The resultant composition and structure of the materials were determined from powder X-Ray diffraction (XRD), Mössbauer spectrometry, thermal analyses and electronic microscopies. The crystalline hydrated fluorides ($\text{MnFeF}_5(\text{H}_2\text{O})_2$ and $\text{MnFe}_2\text{F}_8(\text{H}_2\text{O})_2$) and the corresponding amorphous oxyfluorides ($\text{MnFeF}_{4.6}\text{O}_{0.2}$ and $\text{MnFe}_2\text{F}_{5.8}\text{O}_{1.1}$) were subsequently evaluated for the first time as OER electrocatalysts in highly acidic (0.5M H_2SO_4) media. Notably, the oxyfluorides featured sustained OER activity at 10 mA/cm² for more than 10 hours and thus, present an important addition to the growing library of earth-abundant alternatives to Ir and Ru oxides.

1 Introduction

Global energy consumption is rapidly increasing in concurrence with expanding population and economic development. Presently, most of the energy demand is met by fossil fuels, whose consumption is not sustainable and contributes to issues such as environmental pollution and global warming. To address these problems, it is vital to replace fossil fuels with renewable energy sources such as solar and wind. However, due to the inherent intermittency of renewables, it is therefore necessary to convert renewable electricity to a storable form of energy.¹⁻⁴ Electrocatalytic water splitting, entailing the hydrogen evolution reaction (HER) at the cathode and oxygen evolution reaction (OER) at the anode, converts electricity into H₂ as storable chemical fuel and green energy vector. Despite their promise as key components in a sustainable energy cycle, water electrolysis systems still have much room for improvement in order to attain economic viability.⁵⁻¹⁰ The overall performance of water electrolyzers is limited by the kinetics of the OER which is a primary bottleneck of the process.^{6,11-13} Furthermore, most OER catalysts that are stable in the acidic electrolytes and used in technologically mature polymer electrolyte membrane (PEM)-based electrolyzers contain Ir or Ru, whose the cost hampers their scalability. To this end, significant efforts have been devoted to develop new acid-stable, cost-effective and efficient catalysts.^{5,6,8,12,14}

In alkaline conditions, transition metal (i.e. Fe, Co, Ni, etc) oxides have shown the most promise and have recently begun to overtake Ir/Ru oxides in terms of performance.^{3,5-7,13-15} However, these materials are not stable in acidic electrolytes. Mn oxides are among the few transition metal-based catalyst materials to function stably in acidic conditions but their activity is generally far behind that of Ir/Ru oxides and more complex catalytic architectures such as polyoxometalates.¹⁶⁻²² Because of this, they serve as an important starting point to rationally explore various modifications to enhance their performance. Against this backdrop, fluorinated Mn based materials are promising candidates as electron-withdrawing fluorine species may serve to modulate the electronic structure and hence, reactivity, of the Mn active sites. The strategy to rationally modulate electronic structure of the catalyst by electron withdrawing/donating has been used successfully before in other contexts and thus, our aim was to extend it to acidic OER.²³⁻²⁶ In the context of OER catalysts, substituting electronegative F⁻ in

1
2
3 place of O^{2-} in oxide materials may render the neighboring sites more electron deficient. A growing area
4
5 of investigations points to how fluoride anions can serve to create relatively electron-poor active sites
6
7 within Co, Ni, and Fe oxides that exhibit high OER performance.²⁷⁻³³ Thus, we moved to extend this
8
9 line of investigations toward new fluorinated Mn-based catalysts which operate in acidic electrolytes.

10
11 Over the past decade, few studies have been published the synthesis and OER activity of Mn-based
12
13 oxyfluoride materials. Kumta and co. have exploited the strategy of solid solution formation for the
14
15 preparation of F doped Mn-based electrocatalysts as $Cu_{1+x}Mn_{1-x}O_4:F$ or $Mn_{1+x}In_xO_2:F$ for OER in acidic
16
17 media utilizing both a theoretical and experimental approach.³⁴⁻³⁶ In 2020, a bifunctional catalyst based
18
19 on fluorinated copper manganese oxide exhibited high performance for the oxygen reduction reaction
20
21 (ORR) as well as the OER in both the acidic as well as basic medium.³⁷

22
23
24 Despite the promise of the studies above, the insertion rate of fluorine in oxides is often limited through
25
26 these synthetic approaches and the precise quantification of F as well as the crystalline structure of the
27
28 F doped materials is not fully resolved. Furthermore, there is still much room to improve in this area to
29
30 displace Ir/Ru oxides as the top performing catalyst materials. In comparison to pure oxides and
31
32 fluorides, the synthesis of oxyfluorides is a challenging task due the difficulty of stabilizing both fluorine
33
34 and oxygen anions despite their similar ionic radii (F 1.31Å, O 1.38Å). In the case of Mn-based
35
36 oxyfluorides, the fluorination of the corresponding metal oxides with XeF_2 or CoF_3 as fluorination
37
38 agents for the preparation of $Sr_2Mn_2O_{5-x}F_{1+x}$ and $LiNi_{0.5}Mn_{1.4}Fe_{0.1}Ti_{0.027}O_{4-x}F_x$ ($x=0-0.3$) respectively
39
40 have been reported.^{38,39} Other classical routes such as solid-state chemistry enabled through reactions at
41
42 high temperatures from ceramic route for the preparation of A_2MnO_3F (A = alkaline and alkali-earth
43
44 metals), high energy ball-milling for the $Mn_6O_8F_{4.5}$ and $Li_{1.9}Mn_{0.95}□_{0.15}O_{2.05}F_{0.95}$ or direct reaction of
45
46 metallic precursors with NH_4F for $Cu_{1.5}Mn_{1.5}O_4:xF$ were also studied.^{34,40-42} Recently, we reported a
47
48 novel two-step strategy to prepare new amorphous $M^{2+}M^{3+}_2F_{8-2x}O_x$ oxyfluorides as cathode materials
49
50 for high-capacity lithium-ion batteries.⁴³ This approach is based on the thermal decomposition of the
51
52 hydrated fluoride $M^{2+}M^{3+}_2F_8(H_2O)_2$. Following this strategy, we report in this work the preparation of a
53
54 new Mn-based oxyfluoride, $MnFeF_{4.6}O_{0.2}$, obtained from the calcination of the hydrated fluoride
55
56 $MnFeF_5(H_2O)_2$ that is prepared by microwave-assisted solvothermal synthesis. These Mn-based
57
58
59
60

1
2
3 catalysts, hydrated fluorides $\text{MnFe}_2\text{F}_8(\text{H}_2\text{O})_2$ and $\text{MnFeF}_5(\text{H}_2\text{O})_2$, and the corresponding oxyfluorides
4 $\text{MnFe}_2\text{F}_{5.8}\text{O}_{1.1}$ and $\text{MnFeF}_{4.6}\text{O}_{0.2}$, were tested for the first time for OER electrocatalysis in acidic
5 conditions, and through a series of initial mechanistic investigations, we have added a first round of
6 insights regarding their limitations and routes for improvement.
7
8
9

10 11 12 **2 Results and discussion**

13
14 As reported recently by our group, Mn-Fe based amorphous oxyfluoride ($\text{MnFe}_2\text{F}_{5.8}\text{O}_{1.1}$) was
15 synthesized by thermal decomposition of the corresponding crystalline hydrated phase ($\text{MnFe}_2\text{F}_8(\text{H}_2\text{O})_2$)
16 obtained by microwave-assisted solvothermal synthesis (see **Table S1, S2, S3 and Figure S1**).⁴³ A
17 similar strategy was applied for $\text{MnFeF}_5(\text{H}_2\text{O})_2$. It must be noted that this material can be prepared by
18 hydrothermal synthesis at 380°C and 193 MPa from a mixture of MnF_2 and FeF_3 in aqueous hydrofluoric
19 acid ($\text{HF}_{10\%}$).⁴⁴ The X-ray diffraction pattern of the synthesized solid material confirms the
20 orthorhombic weberite-type phase (space group *Imma*) with a minor MnF_2 impurity, estimated to be 2.9
21 weight percent from Rietveld refinement. Good reliability factors are obtained and the refined atomic
22 positions and the cell parameters of $\text{MnFeF}_5(\text{H}_2\text{O})_2$ are in good agreement with the literature data (ICSD-
23 62362, $a = 7.563(1) \text{ \AA}$, $b = 10.901(2) \text{ \AA}$, $c = 6.732(1) \text{ \AA}$, $V = 555.1 \text{ \AA}^3$). Details of the structure
24 determinations and the atomic positions are given in **Table S1 and S2** and Rietveld pattern is presented
25 in **Figure 1a**). Mössbauer analysis was carried out to gain insight of the iron environment. Mössbauer
26 spectra at 300K and 77K exhibit a paramagnetic structure and were well described by means of a single
27 quadrupolar doublet component. According to the values of their isomer shifts (**Table S3**), they are
28 clearly ascribed to high spin Fe^{3+} species in octahedral coordination (**Figure 1b**) and are in good
29 agreement with these encountered in the weberite structure in which a magnetic frustration appears.^{44,45}
30
31
32
33
34
35
36
37
38
39
40
41
42
43
44
45
46
47
48
49
50
51
52
53
54
55
56
57
58
59
60

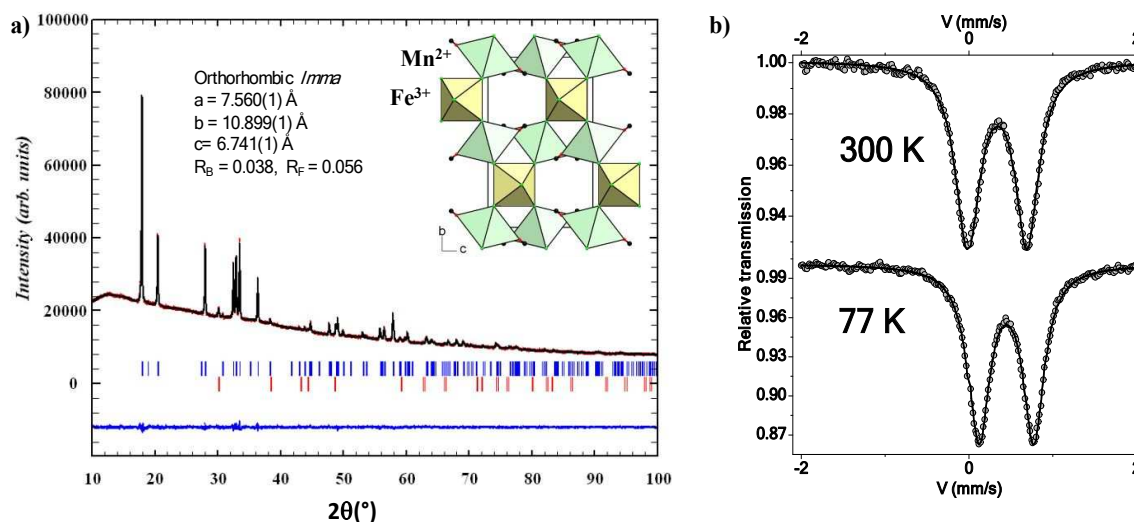


Figure 1. Final Rietveld profile refinement of X-ray powder diffraction pattern (a) and ^{57}Fe Mössbauer spectra at 300K and 77K (b) of $\text{MnFeF}_5(\text{H}_2\text{O})_2$.

The structural evolution with the temperature was first monitored by thermodiffraction under an air environment (**Figure 2a**). Three domains are identified: hydrated crystallized phases (in blue), amorphous intermediate (in green) and crystallized oxides at higher temperatures (in red). The structure of the hydrated fluoride is stable up to 160°C and transforms at 180°C into an amorphous phase. During this crystalline-amorphous phase transition, the shift of the Bragg peak position and the intensity decrease are compatible with the elimination of water and/or HF molecules observed by thermogravimetric analysis coupled with a Mass Spectrometer (TGA-SM) (**Figure 2b**). Finally, at high temperature, the hydrolysis of the amorphous oxyfluoride, in which an oxidation of Mn^{2+} into Mn^{3+} ions occurs, results in the formation of the corundum structure $\text{Mn}^{3+}_{0.5}\text{Fe}^{3+}_{0.5}\text{O}_3$. TGA-MS was further used to determine the composition of the intermediate oxyfluoride, $\text{MnFe}_2\text{F}_{5.8}\text{O}_{1.1}$. As already described for $\text{M}^{2+}\text{Fe}_2^{3+}\text{F}_8(\text{H}_2\text{O})_2$ materials (**Figure S2**), the first weight loss value of thermogravimetry is not compatible with a simple dehydration and is independent of the gaseous atmosphere (air or N_2) (**Figure S3**). Indeed, the water molecules, released during the decomposition of hydrated phase, simultaneously react with the dihydrated fluoride phase to produce HF. This phenomenon is clearly evidenced by TGA-MS under N_2 . The identification of the mass fragments ($m/z = 17$ (OH^+), 18 (H_2O^+), 19 (F^+)) confirms the simultaneous emissions of H_2O and HF molecules (**Figure 2b**). Taking into account the first weight

loss value and the decomposition process, the formulation of this new oxyfluoride can be determined as $\text{MnFeF}_{4.6}\text{O}_{0.2}$ from the following decomposition process:

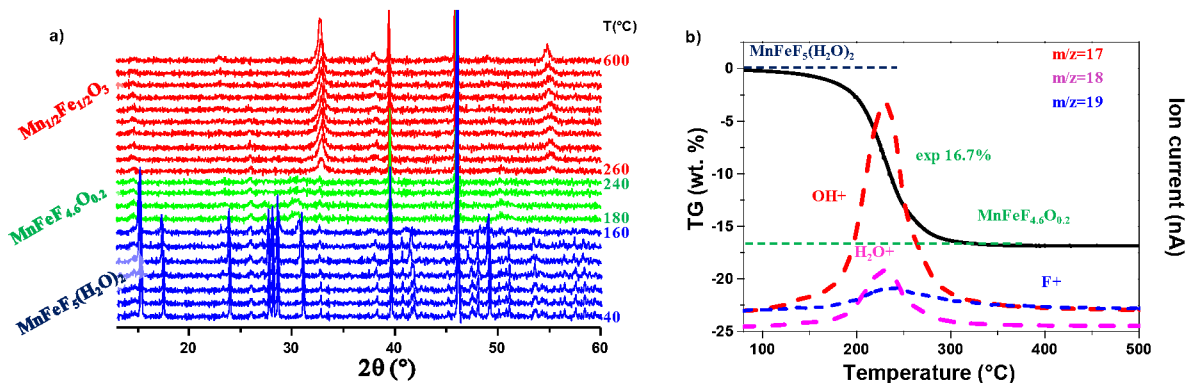
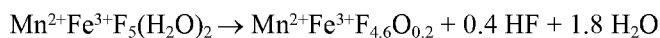


Figure 2. a) Thermal evolution of the X-ray diffractograms under air and b) TGA-MS analyses under N_2 of

$\text{MnFeF}_5(\text{H}_2\text{O})_2$.

This new oxyfluoride intermediate, $\text{MnFeF}_{4.6}\text{O}_{0.2}$, was isolated by calcination of $\text{MnFeF}_5(\text{H}_2\text{O})_2$ under air for 1 h at 220 °C and was characterized by electron microscopies (SEM and TEM, **Figure 3**). The amorphous state of homogenous microsized rods (length: 1–3 μm) is confirmed by the diffuse electron diffraction pattern obtained by selected area electron diffraction (SAED). In addition to the amorphization, this thermal treatment seems to induce a nanostructuration as observed in the TEM images (**Figure 3b, c**). This phenomenon, already observed for $\text{MnFe}_2\text{F}_{5.8}\text{O}_{1.1}$ (**Figure S4 and S5**), is related to the hydrated fluorinated phase decomposition with the dual release of HF and H_2O gases acting as self-generated porogens.^{27,46} Energy dispersive spectroscopy (EDS-SEM, **Figure S6**) elemental mapping provided evidence of the homogenous distribution of both Mn and Fe as well as the Mn/Fe atomic ratio which was found to be close to 1.

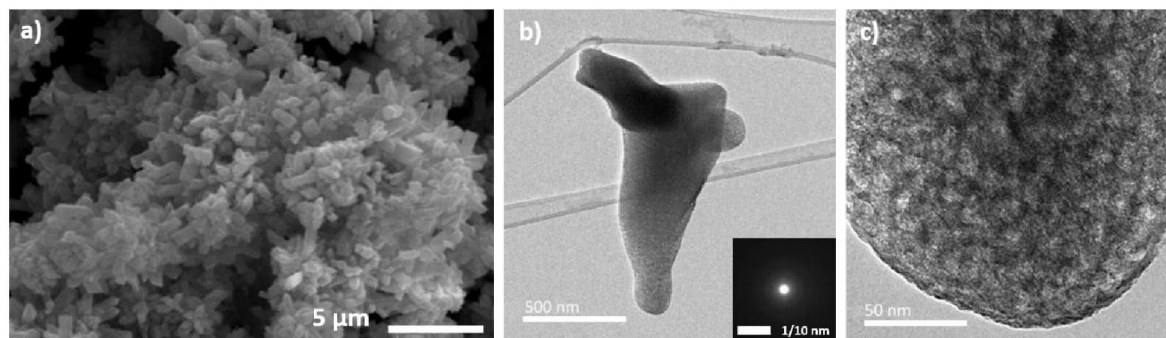


Figure 3: a) SEM and b) and c) TEM images of $\text{MnFeF}_{4.6}\text{O}_{0.2}$ obtained after calcination of $\text{MnFeF}_5(\text{H}_2\text{O})_2$. Inset of b): Corresponding SAED.

2.1 Electrocatalysis

Following the synthesis and characterization of our target materials, we moved to investigate their performance as OER catalysts in acidic conditions. As mentioned earlier, the list of earth-abundant acid stable OER catalysts is much smaller in comparison to the number of earth-abundant alkaline OER catalysts. We proceeded to test both, the hydrated phases, $\text{MnFeF}_5(\text{H}_2\text{O})_2$ and $\text{MnFe}_2\text{F}_8(\text{H}_2\text{O})_2$, and their corresponding amorphous oxyfluorides, $\text{MnFeF}_{4.6}\text{O}_{0.2}$ and $\text{MnFe}_2\text{F}_{5.8}\text{O}_{1.1}$.

To generate functional electrodes from the Mn-based materials, electrodes were first fabricated by mixing the Mn catalyst with carbon nanotubes (CNTs) as a conductive support and a nafion binder in a water:ethanol (50:50 vol%) solvent. This catalyst ink was then drop cast onto a carbon paper electrode and dried under ambient conditions. As a control, electrocatalytic testing was also performed with an electrode comprised of CNTs drop cast onto carbon paper. At first, cyclic voltammetry (CV) was utilized to test the catalytic efficiency of each catalyst (**Figure 4**). In 0.5 M H_2SO_4 electrolyte solution, each material exhibited a reversible redox wave centered around 1.37 V vs. RHE prior to water oxidation catalysis. This likely corresponds to the Mn (II/III) redox couple. In each catalyst, the similarity in the position of the redox wave and OER kinetics points to likely similar physical and electronic structure of the active sites within each material. The width of the catalytic wave ($>1.6\text{V}$) suggests that each of the catalysts features slower water oxidation in the reverse scan (20 mV/sec. scan rate). This observation is perhaps due to a relatively rapid initial adsorption of OER intermediates in the forward scan (in the

positive direction) while the reverse scan (in the negative direction) is more indicative of steady state behavior in which one of the later steps in the OER cycle is rate limiting.

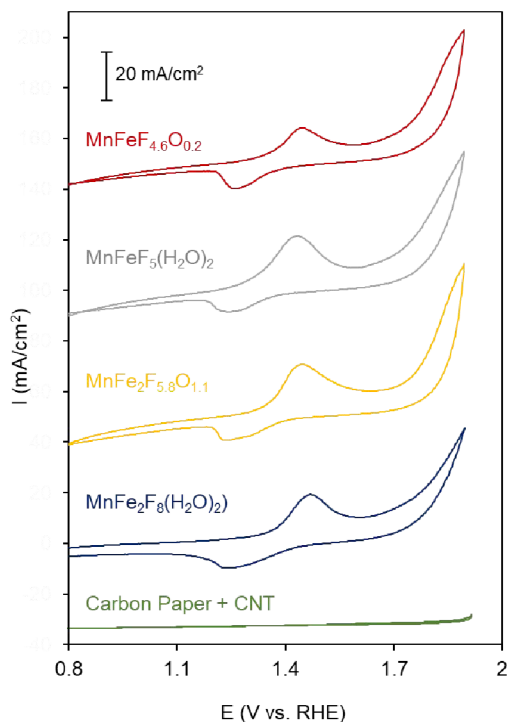


Figure 4: CVs of Mn-based fluorinated materials in 0.5 M H₂SO₄ electrolyte at 20 mV/sec. scan rate.

The stability of each material in H₂SO₄ was subsequently tested through chronopotentiometric scans at 10 mA/cm² (**Figure 5**). Typically, the voltage required to maintain this current density plateaued at 1.8–2 V for several hours, followed by a sharp rise once the catalyst deactivated and at which point the scan was terminated. The oxyfluoride materials, in particular, feature stability comparable with state-of-the-art Mn-based materials reported in the literature.^{18–22,47,48} The crystalline hydrated materials deactivate earlier likely due to their weaker bonding within their structure and are therefore more prone to rapid dissolution.

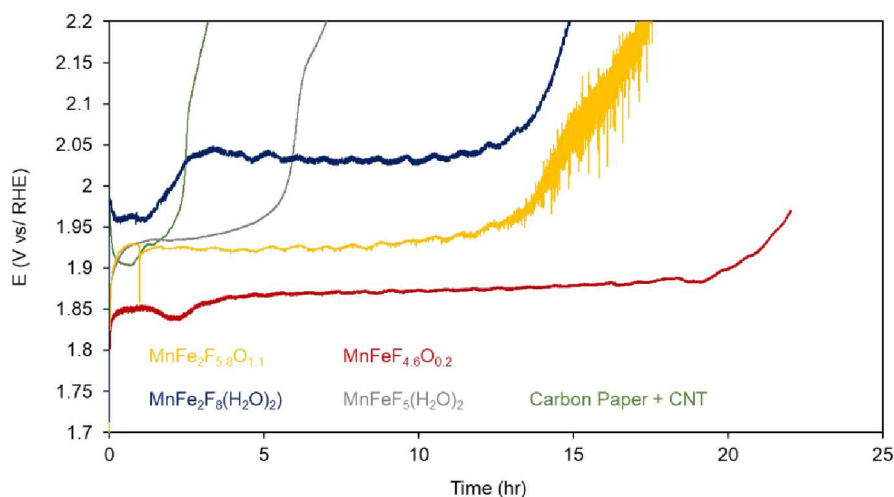


Figure 5 : Chronopotentiometric scans of each Mn material at 10 mA/cm² in 0.5 M H₂SO₄ electrolyte.

Following chronoamperometric scans for 5 hrs at 10 mA/cm², energy-dispersive x-ray spectroscopy - SEM (EDS-SEM) was conducted on the two hydrated crystalline fluorides, MnFeF₅(H₂O)₂ and MnFe₂F₈(H₂O)₂, and their corresponding amorphous oxyfluorides, MnFeF_{4.6}O_{0.2} and MnFe₂F_{5.8}O_{1.1}. In the case of the MnFeF₅(H₂O)₂ and MnFe₂F₈(H₂O)₂ crystalline fluoride phases, complete metal leaching occurred as almost no signal for Mn or Fe were observed after catalysis (**Figure S7**). Only the signal corresponding to fluorine was detected. This points to a structural instability of the hydrated materials under OER conditions over this time frame. However, the corresponding oxyfluorides seemed to be more stable under acid. Indeed, Mn and F are still present in both cases (**Figure S8**). The leaching of the Fe throughout the reaction points to the Mn species being the likely active site within the material and that the Fe does not particularly dictate the activity like it does with Ni-Fe oxides in alkaline OER studies.⁴⁹ With this observation, we can postulate that a porous Mn oxyfluoride serves as the OER active phase within our amorphous materials.

Taking MnFeF_{4.6}O_{0.2} as a case study to probe the rate limiting step of the OER reaction, we turned to electrochemical nucleophile oxidation. The oxidation of nucleophiles such as methanol occurs once the surface of the catalyst becomes covered with electrophilic intermediates like *OH.⁵⁰ As such, an enhancement of current in the presence of a nucleophile indicates that the rate limiting step is not the first adsorption to generate *OH but rather one of the later steps such as the formation of *O or *OOH.

1
2
3 The enhancement of current at the onset of the oxidation of the Mn^{2+} (**Figure S9**) indicates that *OH
4 readily forms once Mn^{3+} is generated, and that once this occurs, the rate limiting step is further down
5 the catalytic cycle. Thus, above 1.4V, the initial deprotonation and surface adsorption of H_2O to
6 generate *OH is likely not rate limiting. When applied as an oxygen reduction reaction (ORR)
7 electrocatalyst in a rotating ring disk setup, $\text{MnFeF}_{4.6}\text{O}_{0.2}$ proceeds almost entirely via the $4e^-$ pathway
8 (**Figure S10**). This is an indication that the $\text{*OOH} \rightarrow \text{*O}$ step features a relatively small reaction barrier
9 in comparison with the desorption of *OOH to generate H_2O_2 in the $2e^-$ pathway. If we assume that the
10 reverse $\text{*O} \rightarrow \text{*OOH}$ step oxygen coupling step also has a relatively small barrier in the OER reaction
11 pathway, then this would indicate that either the $\text{*OH} \rightarrow \text{*O}$ or $\text{*OOH} \rightarrow \text{*OO}$ is the rate limiting step.
12 To this end, having proton acceptor species, either within the electrolyte or on the catalyst surface may
13 boost the Mn oxyfluorides' OER performance. However, this is not yet fully conclusive and further
14 experiments and theoretical calculations would be helpful to verify and further explore the mechanisms
15 of Mn oxyfluoride acidic OER.
16
17
18
19
20
21
22
23
24
25
26
27
28

29 As a new class of earth-abundant OER materials is unveiled in this work, it would be worthwhile
30 to follow up in the directions of both, mechanistic studies and systematic improvement of
31 activity/stability. The investigation of precisely how starting composition influences both activity and
32 stability stand to yield critical design criteria towards the development of next-generation acid-stable
33 OER materials. Further, *in situ* spectroscopic techniques such as infrared or X-ray absorption
34 spectroscopy can elucidate the precise chemical nature of the active site and reaction intermediates under
35 reaction conditions and thus are a promising future route of investigation. This would be key to link how
36 the starting structure evolves to the catalytically active phase. Further, as the exact catalytic active
37 site(s)' structure is still undetermined, theoretical calculations would be highly beneficial to screen
38 several candidate structures with the aim of maximizing such motifs in the next generation of materials.
39
40
41
42
43
44
45
46
47
48
49

50 **3 Conclusions**

51
52 In conclusion, through expanding our established synthetic strategy for the synthesis manganese
53 based fluorinated materials ($\text{MnFe}_2\text{F}_8(\text{H}_2\text{O})_2$ and $\text{MnFe}_2\text{F}_{5.8}\text{O}_{1.1}$), a new oxyfluoride $\text{MnFeF}_{4.6}\text{O}_{0.2}$ was
54 obtained through a thermal treatment under air of the metal mixed hydrated fluoride $\text{MnFeF}_5(\text{H}_2\text{O})_2$.
55
56
57
58
59
60

1
2
3 The resultant fluorinated material was characterized with a combination of TGA, TGA-MS, HT-DRX
4 and EDS-SEM and it was found that the calcination induces both amorphization and nanostructuration
5 of the oxyfluoride. The full series of crystalline hydrated fluorides ($\text{MnFeF}_5(\text{H}_2\text{O})_2$ and $\text{MnFe}_2\text{F}_8(\text{H}_2\text{O})_2$)
6 and their corresponding amorphous oxyfluorides ($\text{MnFeF}_{4.6}\text{O}_{0.2}$ and $\text{MnFe}_2\text{F}_{5.8}\text{O}_{1.1}$) were investigated as
7 OER catalysts in acidic conditions. The amorphous manganese oxyfluorides featured substantial
8 stability in highly acidic conditions and thus add to a comparatively small but growing class of catalyst
9 materials aiming to take the place of Ir/Ru oxides in PEM-based electrolyzers. Importantly, this study
10 opens many routes on which to build upon to understand and improve Mn-based OER electrocatalysts.
11 These preliminary results encourage attempts to synthesize other oxyfluorides $\text{Mn}^{2+}_x\text{M}^{3+}_{1-x}\text{O}_{1-x}\text{F}_{1+x}$
12 materials with various compositions modulating the electrocatalysts properties to better understand the
13 effect of the chemical compositions (F/O and Mn/ M^{3+} ratios) on the OER performance as well as in-
14 depth mechanistic studies in order to determine the most efficient active site motifs within these
15 amorphous Mn oxyfluorides.
16
17
18
19
20
21
22
23
24
25
26
27
28

29 **4 Materials and synthesis methods**

30
31
32 The hydrated fluorides, $\text{MnFeF}_5(\text{H}_2\text{O})_2$ and $\text{MnFe}_2\text{F}_8(\text{H}_2\text{O})_2$, were obtained by microwave-assisted
33 solvothermal reaction using a MARS-5 microwave Digestion System (CEM Corp.) starting from
34 chloride precursors (Alfa Aesar), 9.45 mL of absolute methanol (MeOH, 233 mmol, $24.7 \text{ mol}\cdot\text{L}^{-1}$,
35 99.8%, Sigma- Aldrich), and 0.55 mL of hydrofluoric acid solution (15 mmol, $27.6 \text{ mol}\cdot\text{L}^{-1}$, Riedel De
36 Haen). For the preparation of $\text{MnFeF}_5(\text{H}_2\text{O})_2$, the $[\text{Mn}^{2+}]+[\text{Fe}^{3+}]$ concentration was fixed to $0.2 \text{ mol}\cdot\text{L}^{-1}$
37 ($n_{\text{Mn}^{2+}} = 1 \text{ mmol}$, $n_{\text{Fe}^{3+}} = 1 \text{ mmol}$) and a ratio $[\text{Mn}^{2+}]/[\text{Fe}^{3+}] = 1$, a volume (HF+MeOH) of 10 mL and a
38 $\text{MnCl}_2/\text{FeCl}_3/\text{HF}/\text{MeOH}$ molar ratio of 1/1/22/350 were used. After microwave heating at 160°C for 1 h
39 with stirring, the white solid product is filtered, washed with ethanol and then dried in an oven in air at
40 100°C overnight. The synthesis of $\text{MnFe}_2\text{F}_8(\text{H}_2\text{O})_2$ was already reported in 2019.⁴³ Briefly, the
41 concentration $[\text{Mn}^{2+}]+[\text{Fe}^{3+}]$ was fixed equal to $0.1 \text{ mol}\cdot\text{L}^{-1}$ and the $\text{Mn}^{2+}/\text{Fe}^{3+}/\text{HF}/\text{MeOH}$ ratio equal to
42 1/2/44/699. The mixture was placed in Teflon autoclaves and heated at 160°C for 30 min with stirring.
43 After cooling, the solid products are filtered, washed with 2 mL of ethanol, and dried in a furnace under
44 air at 100°C overnight.
45
46
47
48
49
50
51
52
53
54
55
56
57
58
59
60

1
2
3 Both hydrated fluorides were used as precursors to obtain the corresponding oxyfluorides by thermal
4 treatment under ambient air at $T = 220^{\circ}\text{C}$ and 340°C for $\text{MnFeF}_5(\text{H}_2\text{O})_2$ and $\text{MnFe}_2\text{F}_8(\text{H}_2\text{O})_2$,
5 respectively (heating/cooling rate of $2^{\circ}\text{C}/\text{min}$). The formulations, $\text{MnFeF}_{4.6}\text{O}_{0.2}$ et $\text{MnFe}_2\text{F}_{5.8}\text{O}_{1.1}$,⁴⁶ were
6 established from thermal analyses (see the following section). After thermal treatment, all phases are
7 immediately out-gassed at ambient temperature under secondary vacuum ($P < 10^{-5}$ bar) and stored in a
8 glovebox. It must be noted that all sample preparations for Mössbauer spectrometry were realized in a
9 glovebox.
10
11
12
13
14
15

16 17 18 **4.1 Characterizations**

19
20 X-ray diffraction patterns were collected in the range $10^{\circ} \leq 2\theta \leq 150^{\circ}$ on a Panalytical MPD-PRO
21 diffractometer equipped with a linear X'celerator detector with $\text{CuK}\alpha$ (1.5406 \AA) anode. Rietveld
22 refinements were performed by using the Fullprof profile refinement program.
23
24
25

26
27 X-ray thermodiffraction (HT-XRD) was performed under dry air in an Anton Parr XRK 900 high
28 temperature furnace with diffractometer described. The samples were heated from 40 to 600°C at a
29 heating rate of $10^{\circ}\text{C}\cdot\text{min}^{-1}$. X-ray diffraction patterns were recorded in the $[5-60^{\circ}]$ 2θ range with a scan
30 time of 10 min at 20°C intervals from room temperature to 400 and at 100°C intervals from 400 to
31 600°C .
32
33
34
35

36
37 Mass Spectroscopy coupled Thermo Gravimetric Analysis (MS-TGA) was performed using a Netzch
38 STA 449 F3 coupled with a QMS 403 C mass spectrometer. The thermoanalytical curves were recorded
39 from room temperature up to 500°C together with the ion current curves in the multiple ions detection
40 probe. A constant purge nitrogen gas flow of $80 \text{ mL}\cdot\text{min}^{-1}$ and a constant heating rate of $5^{\circ}\text{C}\cdot\text{min}^{-1}$ were
41 applied. The thermogravimetric (TGA) experiments under air (Alphagaz, mixture of oxygen (20%) with
42 nitrogen (80%), $\text{H}_2\text{O} < 3 \text{ ppm}$) were carried out with a thermoanalyzer SETARAM TGA 92 with a
43 heating rate of $5^{\circ}\text{C}\cdot\text{min}^{-1}$ from room temperature up to 600°C .
44
45
46
47
48
49
50

51
52 SEM images were obtained using a JEOL microscope (JSM 6510 LV). Acceleration voltages varied
53 between 20 and 30 kV as a function of the analyzed samples. Elementary quantitative microanalyses
54 were performed using an Energy Dispersive X-ray (EDX) OXFORD detector (AZtec software).
55
56
57
58
59
60

1
2
3 The TEM was conducted on a JEOL JEM 2100 HR electron microscope operating at 200 kV and
4 equipped with a side entry $\pm 35^\circ$ double-tilt specimen holder. The sample for transmission electron
5 microscopy investigation were prepared by ultrasonically dispersing the raw powder in ethanol,
6 depositing a drop of the resulting suspension onto a holey carbon-coated copper grid and finally drying
7 the grid in air.
8
9
10
11
12

13 Mössbauer measurements were performed in transmission geometry with a 925 MBq γ -source of
14 $^{57}\text{Co}/\text{Rh}$ mounted on a conventional constant acceleration drive. The samples with $5 \text{ mg of Fe}\cdot\text{cm}^{-2}$
15 were prepared from a softly milled powder. Data were fitted using the MOSFIT program³⁷ involving
16 quadrupolar and/or magnetic components with Lorentzian lines; the isomer shift values are referred to
17 that of α -Fe at RT. The velocity of the source was calibrated using α -Fe as the standard at room
18 temperature.
19
20
21
22
23
24
25

26 **Electrochemical measurements:**

27
28
29 Catalyst inks were first created by sonicating for 20 min approximately 10 mg of the desired Mn-
30 Fe fluorides powder with 0.5 mg of carbon nanotubes (40 nm, multiwalled, Sigma Aldrich) in 1 mL of
31 a 50:50 ethanol:water (vol:vol) with 50 μL of 5% nafion solution added. This catalyst ink was then drop
32 cast onto either Toray Carbon Paper (for OER) or glassy carbon (for oxygen reduction) to attain a
33 catalyst loading of $1 \text{ mg}/\text{cm}^2$ and was dried in an air environment at 80°C . Electrochemical
34 measurements were primarily performed with custom-built 2 compartment electrochemical cells and
35 Ag/AgCl and graphite rod electrodes were used as reference and counter electrodes. Typically, a
36 Biologic VMP200 was used for electrochemical experiments. IR drop compensation (85%) was
37 performed with the EC-lab ZIR function by measuring the impedance at 100 KHz at open circuit.
38
39
40
41
42
43
44
45
46
47

48 **Acknowledgments**

49
50
51 The authors give thanks to French Research Ministry for a doctoral grant. The authors attached to the
52 IMMM institute to gratefully acknowledge the "X-ray Diffusion and Diffraction" and the "Electron
53 Microscopy" technical platforms of IMMM (Le Mans University). J.L. thanks CNRS for funding the
54
55
56
57
58
59
60

EMERGENCE@INC2020 Project (H₂FLU). N.K. and N.H. acknowledge the NSERC Discovery Grant RGPIN-2019-05927. All authors thank to FRQNT Samuel de Champlain program, award 293526.

References

- (1) Hoffert, M. I.; Caldeira, K.; Jain, A. K.; Haites, E. F.; Harvey, L. D. D.; Potter, S. D.; Schlesinger, M. E.; Schneider, S. H.; Watts, R. G.; Wigley, T. M. L.; Wuebbles, D. J. Energy Implications of Future Stabilization of Atmospheric CO₂ Content. *Nature* **1998**, *395* (6705), 881–884. <https://doi.org/10.1038/27638>.
- (2) Nejat, P.; Jomehzadeh, F.; Taheri, M. M.; Gohari, M.; Muhd, M. Z. A Global Review of Energy Consumption, CO₂ Emissions and Policy in the Residential Sector (with an Overview of the Top Ten CO₂ Emitting Countries). *Renew. Sustain. Energy Rev.* **2015**, *43*, 843–862. <https://doi.org/10.1016/j.rser.2014.11.066>.
- (3) Hu, C.; Zhang, L.; Gong, J. Recent Progress Made in the Mechanism Comprehension and Design of Electrocatalysts for Alkaline Water Splitting. *Energy Environ. Sci.* **2019**, *12* (9), 2620–2645. <https://doi.org/10.1039/c9ee01202h>.
- (4) Trotochaud, L.; Ranney, J. K.; Williams, K. N.; Boettcher, S. W. Solution-Cast Metal Oxide Thin Film Electrocatalysts for Oxygen Evolution. *J. Am. Chem. Soc.* **2012**, *134* (41), 17253–17261. <https://doi.org/10.1021/ja307507a>.
- (5) Dionigi, F.; Strasser, P. NiFe-Based (Oxy)Hydroxide Catalysts for Oxygen Evolution Reaction in Non-Acidic Electrolytes. *Advanced Energy Materials*. Wiley-VCH Verlag December 7, 2016. <https://doi.org/10.1002/aenm.201600621>.
- (6) Zhou, D.; Wang, S.; Jia, Y.; Xiong, X.; Yang, H.; Liu, S.; Tang, J.; Zhang, J.; Liu, D.; Zheng, L.; Kuang, Y.; Sun, X.; Liu, B. NiFe Hydroxide Lattice Tensile Strain: Enhancement of Adsorption of Oxygenated Intermediates for Efficient Water Oxidation Catalysis. *Angew. Chemie - Int. Ed.* **2019**, *58* (3), 736–740. <https://doi.org/10.1002/anie.201809689>.
- (7) Ou, G.; Wu, F.; Huang, K.; Hussain, N.; Zu, D.; Wei, H.; Ge, B.; Yao, H.; Liu, L.; Li, H.; Shi,

- 1
2
3 Y.; Wu, H. Boosting the Electrocatalytic Water Oxidation Performance of CoFe_2O_4
4 Nanoparticles by Surface Defect Engineering. *ACS Appl. Mater. Interfaces* **2019**, *11* (4), 3978–
5 3983. <https://doi.org/10.1021/acsami.8b19265>.
6
7
8
9
10 (8) Wang, H.; Lee, H. W.; Deng, Y.; Lu, Z.; Hsu, P. C.; Liu, Y.; Lin, D.; Cui, Y. Bifunctional Non-
11 Noble Metal Oxide Nanoparticle Electrocatalysts through Lithium-Induced Conversion for
12 Overall Water Splitting. *Nat. Commun.* **2015**, *6* (7261), 1–8.
13 <https://doi.org/10.1038/ncomms8261>.
14
15
16
17
18 (9) Fan, K.; Chen, H.; Ji, Y.; Huang, H.; Claesson, P. M.; Daniel, Q.; Philippe, B.; Rensmo, H.; Li,
19 F.; Luo, Y.; Sun, L. Nickel-Vanadium Monolayer Double Hydroxide for Efficient
20 Electrochemical Water Oxidation. *Nat. Commun.* **2016**, *7* (11981), 1–9.
21 <https://doi.org/10.1038/ncomms11981>.
22
23
24
25
26
27 (10) Hui, L.; Xue, Y.; Huang, B.; Yu, H.; Zhang, C.; Zhang, D.; Jia, D.; Zhao, Y.; Li, Y.; Liu, H.; Li,
28 Y. Overall Water Splitting by Graphdiyne-Exfoliated and -Sandwiched Layered Double-
29 Hydroxide Nanosheet Arrays. *Nat. Commun.* **2018**, *9* (5309), 1–11.
30 <https://doi.org/10.1038/s41467-018-07790-x>.
31
32
33
34
35
36 (11) Indra, A.; Menezes, P. W.; Sahraie, N. R.; Bergmann, A.; Das, C.; Tallarida, M.; Schmeißer, D.;
37 Strasser, P.; Driess, M. Unification of Catalytic Water Oxidation and Oxygen Reduction
38 Reactions: Amorphous Beat Crystalline Cobalt Iron Oxides. *J. Am. Chem. Soc.* **2014**, *136* (50),
39 17530–17536. <https://doi.org/10.1021/ja509348t>.
40
41
42
43
44 (12) Pittkowski, R.; Krtil, P.; Rossmeisl, J. Rationality in the New Oxygen Evolution Catalyst
45 Development. *Curr. Opin. Electrochem.* **2018**, *12*, 218–224.
46 <https://doi.org/10.1016/j.coelec.2018.11.014>.
47
48
49
50
51 (13) Lyons, M. E. G.; Doyle, R. L.; Browne, M. P.; Godwin, I. J.; Rovetta, A. A. S. Recent
52 Developments in Electrochemical Water Oxidation. *Curr. Opin. Electrochem.* **2017**, *1*, 40–45.
53 <https://doi.org/10.1016/j.coelec.2016.12.005>.
54
55
56
57
58
59
60

- 1
2
3 (14) Wallace, A. G.; Symes, M. D. Water-Splitting Electrocatalysts Synthesized Using Ionic Liquids.
4 *Trends Chem.* **2019**, *1* (2), 247–258. <https://doi.org/10.1016/j.trechm.2019.03.003>.
5
6
7 (15) Godwin, I.; Rovetta, A.; Lyons, M.; Coleman, J. Electrochemical Water Oxidation: The next
8 Five Years. *Curr. Opin. Electrochem.* **2018**, *7*, 31–35.
9 <https://doi.org/10.1016/j.coelec.2017.09.025>.
10
11
12
13
14 (16) Park, S.; Lee, Y. H.; Choi, S.; Seo, H.; Lee, M. Y.; Balamurugan, M.; Nam, K. T. Manganese
15 Oxide-Based Heterogeneous Electrocatalysts for Water Oxidation. *Energy Environ. Sci.* **2020**,
16 *13* (8), 2310–2340. <https://doi.org/10.1039/d0ee00815j>.
17
18
19
20
21 (17) Li, A.; Ooka, H.; Bonnet, N.; Hayashi, T.; Sun, Y.; Jiang, Q.; Li, C.; Han, H.; Nakamura, R.
22 Stable Potential Windows for Long-Term Electrocatalysis by Manganese Oxides Under Acidic
23 Conditions. *Angew. Chemie Int. Ed.* **2019**, *58* (15), 5054–5058.
24 <https://doi.org/10.1002/anie.201813361>.
25
26
27
28
29
30 (18) Zhou, L.; Shinde, A.; Montoya, J. H.; Singh, A.; Gul, S.; Yano, J.; Ye, Y.; Crumlin, E. J.; Richter,
31 M. H.; Cooper, J. K.; Stein, H. S.; Haber, J. A.; Persson, K. A.; Gregoire, J. M. Rutile Alloys in
32 the Mn-Sb-O System Stabilize Mn³⁺ to Enable Oxygen Evolution in Strong Acid. *ACS Catal.*
33 **2018**, *8* (12), 10938–10948. <https://doi.org/10.1021/acscatal.8b02689>.
34
35
36
37
38 (19) Huynh, M.; Bediako, D. K.; Nocera, D. G. A Functionally Stable Manganese Oxide Oxygen
39 Evolution Catalyst in Acid. *J. Am. Chem. Soc.* **2014**, *136* (16), 6002–6010.
40 <https://doi.org/10.1021/ja413147e>.
41
42
43
44
45 (20) Maayan, G.; Gluz, N.; Christou, G. A Bioinspired Soluble Manganese Cluster as a Water
46 Oxidation Electrocatalyst with Low Overpotential. *Nat. Catal.* **2018**, *1*, 48–54.
47 <https://doi.org/10.1038/s41929-017-0004-2>.
48
49
50
51 (21) Huynh, M.; Ozel, T.; Liu, C.; Lau, E. C.; Nocera, D. G. Design of Template-Stabilized Active
52 and Earth-Abundant Oxygen Evolution Catalysts in Acid. *Chem. Sci.* **2017**, *8* (7), 4779–4794.
53 <https://doi.org/10.1039/c7sc01239j>.
54
55
56
57
58
59
60

- 1
2
3 (22) Blasco-Ahicart, M.; Soriano-Lopez, J.; Carbo, J. J.; Poblet, J. M.; Galan-Mascaros, J. R.
4 Polyoxometalate Electrocatalysts Based on Earthabundant Metals for Efficient Water Oxidation
5 in Acidic Media. *Nat. Chem.* **2018**, *10* (1), 24–30. <https://doi.org/10.1038/NCHEM.2874>.
6
7
8
9 (23) Kuznetsov, D. A.; Han, B.; Yu, Y.; Rao, R. R.; Hwang, J.; Román-Leshkov, Y.; Shao-Horn, Y.
10 Tuning Redox Transitions via Inductive Effect in Metal Oxides and Complexes, and Implications
11 in Oxygen Electrocatalysis. *Joule* **2018**, *2*, 225–244. <https://doi.org/10.1016/j.joule.2017.11.014>.
12
13
14
15 (24) Kornienko, N. Enhancing Catalysis through Substitute-Driven Redox Tuning. *Joule* **2018**, *2*,
16 207–209. <https://doi.org/10.1016/j.joule.2018.01.005>.
17
18
19 (25) Zagal, J. H.; Koper, M. T. M. Reactivity Descriptors for the Activity of Molecular MN_4 Catalysts
20 for the Oxygen Reduction Reaction. *Angew. Chemie Int. Ed.* **2016**, *55* (47), 14510–14521.
21 <https://doi.org/10.1002/anie.201604311>.
22
23
24 (26) Yang, W.; Wang, Z.; Zhang, W.; Guo, S. Electronic-Structure Tuning of Water-Splitting
25 Nanocatalysts. *Trends Chem.* **2019**, *1* (2), 259–271.
26 <https://doi.org/10.1016/j.trechm.2019.03.006>.
27
28
29 (27) Lemoine, K.; Lhoste, J.; Hémon-Ribaud, A.; Heidary, N.; Maisonneuve, V.; Guiet, A.;
30 Kornienko, N. Investigation of Mixed-Metal (Oxy)Fluorides as a New Class of Water Oxidation
31 Electrocatalysts. *Chem. Sci.* **2019**, *10* (40), 9209–9218. <https://doi.org/10.1039/c9sc04027g>.
32
33
34 (28) Liang, K.; Guo, L.; Marcus, K.; Zhang, S.; Yang, Z.; Perea, D. E.; Zhou, L.; Du, Y.; Yang, Y.
35 Overall Water Splitting with Room-Temperature Synthesized NiFe Oxyfluoride Nanoporous
36 Films. *ACS Catal.* **2017**, *7* (12), 8406–8412. <https://doi.org/10.1021/acscatal.7b02991>.
37
38
39 (29) Fan, X.; Liu, Y.; Chen, S.; Shi, J.; Wang, J.; Fan, A.; Zan, W.; Li, S.; Goddard, W. A.; Zhang,
40 X. M. Defect-Enriched Iron Fluoride-Oxide Nanoporous Thin Films Bifunctional Catalyst for
41 Water Splitting. *Nat. Commun.* **2018**, *9* (1809), 1–11. <https://doi.org/10.1038/s41467-018-04248-y>.
42
43
44 (30) Chen, P.; Zhou, T.; Wang, S.; Zhang, N.; Tong, Y.; Ju, H.; Chu, W.; Wu, C.; Xie, Y. Dynamic
45
46
47
48
49
50
51
52
53
54
55
56
57
58
59
60

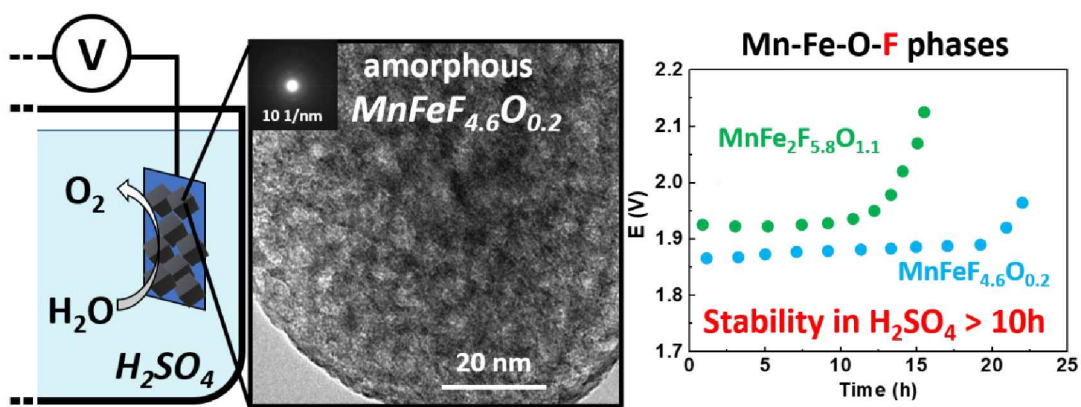
- 1
2
3 Migration of Surface Fluorine Anions on Cobalt-Based Materials to Achieve Enhanced Oxygen
4 Evolution Catalysis. *Angew. Chemie Int. Ed.* **2018**, *57* (47), 15471–15475.
5
6 <https://doi.org/10.1002/anie.201809220>.
7
8
9 (31) Xue, Y.; Wang, Y.; Liu, H.; Yu, X.; Xue, H.; Feng, L. Electrochemical Oxygen Evolution
10 Reaction Catalyzed by a Novel Nickel-Cobalt-Fluoride Catalyst. *Chem. Commun.* **2018**, *54* (48),
11 6204–6207. <https://doi.org/10.1039/c8cc03223h>.
12
13
14
15 (32) Han, H.; Woo, J.; Hong, Y. R.; Chung, Y. C.; Mhin, S. Polarized Electronic Configuration in
16 Transition Metal-Fluoride Oxide Hollow Nanoprism for Highly Efficient and Robust Water
17 Splitting. *ACS Appl. Energy Mater.* **2019**, *2* (6), 3999–4007.
18
19 <https://doi.org/10.1021/acsaem.9b00449>.
20
21
22
23 (33) Pei, C.; Chen, H.; Dong, B.; Yu, X.; Feng, L. Electrochemical Oxygen Evolution Reaction
24 Efficiently Catalyzed by a Novel Porous Iron-Cobalt-Fluoride Nanocube Easily Derived from 3-
25 Dimensional Prussian Blue Analogue. *J. Power Sources* **2019**, *424*, 131–137.
26
27 <https://doi.org/10.1016/j.jpowsour.2019.03.089>.
28
29
30
31 (34) Patel, P. P.; Datta, M. K.; Velikokhatnyi, O. I.; Kuruba, R.; Damodaran, K.; Jampani, P.; Gattu,
32 B.; Shanthi, P. M.; Damle, S. S.; Kumta, P. N. Noble Metal-Free Bifunctional Oxygen Evolution
33 and Oxygen Reduction Acidic Media Electro-Catalysts. *Sci. Rep.* **2016**, *6* (1), 1–14.
34
35 <https://doi.org/10.1038/srep28367>.
36
37
38
39 (35) Ghadge, S. D.; Patel, P. P.; Datta, M. K.; Velikokhatnyi, O. I.; Kuruba, R.; Shanthi, P. M.; Kumta,
40 P. N. Fluorine Substituted (Mn,Ir)O₂:F High Performance Solid Solution Oxygen Evolution
41 Reaction Electro-Catalysts for PEM Water Electrolysis. *RSC Adv.* **2017**, *7* (28), 17311–17324.
42
43 <https://doi.org/10.1039/c6ra27354h>.
44
45
46
47 (36) Ghadge, S. D.; Velikokhatnyi, O. I.; Datta, M. K.; Shanthi, P. M.; Tan, S.; Damodaran, K.;
48 Kumta, P. N. Experimental and Theoretical Validation of High Efficiency and Robust
49 Electrocatalytic Response of One-Dimensional (1D) (Mn,Ir)O₂:10F Nanorods for the Oxygen
50
51
52
53
54
55
56
57
58
59
60

- 1
2
3 Evolution Reaction in PEM-Based Water Electrolysis. *ACS Catal.* **2019**, *9* (3), 2134–2157.
4 <https://doi.org/10.1021/acscatal.8b02901>.
5
6
7
8 (37) Rai, V.; Lee, K. P.; Safanama, D.; Adams, S.; Blackwood, D. J. Oxygen Reduction and Evolution
9 Reaction (ORR and OER) Bifunctional Electrocatalyst Operating in Wide PH Range for
10 Cathodic Application in Li-Air Battery. *ACS Appl. Energy Mater.* **2020**, *xx*, xx–xx.
11 <https://doi.org/10.1021/acsaem.0c01775>.
12
13
14
15
16 (38) Lobanov, M. V.; Abakumov, A. M.; Sidorova, A. V.; Rozova, M. G.; D'yachenko, O. G.;
17 Antipov, E. V.; Hadermann, J.; Van Tendeloo, G. Synthesis and Investigation of Novel Mn-
18 Based Oxyfluoride $\text{Sr}_2\text{Mn}_2\text{O}_{5-x}\text{F}_{1+x}$. *Solid State Sci.* **2002**, *4* (1), 19–22.
19 [https://doi.org/10.1016/S1293-2558\(01\)01209-2](https://doi.org/10.1016/S1293-2558(01)01209-2).
20
21
22
23
24
25 (39) Höweling, A.; Stenzel, D.; Gesswein, H.; Kaus, M.; Indris, S.; Bergfeldt, T.; Binder, J. R.
26 Variations in Structure and Electrochemistry of Iron- and Titanium-Doped Lithium Nickel
27 Manganese Oxyfluoride Spinel. *J. Power Sources* **2016**, *315*, 269–276.
28 <https://doi.org/10.1016/j.jpowsour.2016.03.023>.
29
30
31
32
33
34 (40) Su, Y.; Tsujimoto, Y.; Matsushita, Y.; Yuan, Y.; He, J.; Yamaura, K. High-Pressure Synthesis,
35 Crystal Structure, and Magnetic Properties of $\text{Sr}_2\text{MnO}_3\text{F}$: A New Member of Layered Perovskite
36 Oxyfluorides. *Inorg. Chem.* **2016**, *55* (5), 2627–2633.
37 <https://doi.org/10.1021/acs.inorgchem.5b02984>.
38
39
40
41
42
43 (41) Zhang, L.; Dambournet, D.; Iadecola, A.; Batuk, D.; Borkiewicz, O. J.; Wiaderek, K. M.;
44 Salager, E.; Shao, M.; Chen, G.; Tarascon, J. M. Origin of the High Capacity Manganese-Based
45 Oxyfluoride Electrodes for Rechargeable Batteries. *Chem. Mater.* **2018**, *30* (15), 5362–5372.
46 <https://doi.org/10.1021/acs.chemmater.8b02182>.
47
48
49
50
51
52 (42) House, R. A.; Jin, L.; Maitra, U.; Tsuruta, K.; Somerville, J. W.; Förstermann, D. P.; Massel, F.;
53 Duda, L.; Roberts, M. R.; Bruce, P. G. Lithium Manganese Oxyfluoride as a New Cathode
54 Material Exhibiting Oxygen Redox. *Energy Environ. Sci.* **2018**, *11* (4), 926–932.
55
56
57
58
59
60

- 1
2
3 <https://doi.org/10.1039/c7ee03195e>.
- 4
5
6 (43) Lemoine, K.; Zhang, L.; Grenèche, J.-M.; Hémon-Ribaud, A.; Leblanc, M.; Guiet, A.; Galven,
7 C.; Tarascon, J.-M.; Maisonneuve, V.; Lhoste, J. New Amorphous Iron-Based Oxyfluorides as
8 Cathode Materials for High-Capacity Lithium-Ion Batteries. *J. Phys. Chem. C* **2019**, *123* (35),
9 21386–21394. <https://doi.org/10.1021/acs.jpcc.9b06055>.
- 10
11
12
13
14 (44) Greneche, J. M.; Linares, J.; Varret, F.; Laligant, Y.; Ferey, G. Mössbauer Spectroscopy of the
15 Magnetic Behaviour of the Frustrated Series $AFeF_5(H_2O)_2$: A = Mn, Fe, Co, Ni. *J. Magn. Magn.*
16 *Mater.* **1988**, *73* (1), 115–122. [https://doi.org/10.1016/0304-8853\(88\)90177-1](https://doi.org/10.1016/0304-8853(88)90177-1).
- 17
18
19
20
21 (45) Albino, M.; Clark, L.; Lhoste, J.; Payen, C.; Grenèche, J.-M.; Lightfoot, P.; Maisonneuve, V.;
22 Leblanc, M. A Magnetisation and Mössbauer Study of Triazole $(M_{1-x}^{2+}M_x^{3+})M^{3+}F_5(Htaz)_1$.
23 $_x(Taz)_x$ Weberites (M = Fe, Co, Mn, Zn, Ga, V). *Dalt. Trans.* **2017**, *46* (16).
24 <https://doi.org/10.1039/c7dt00587c>.
- 25
26
27
28
29
30 (46) Lemoine, K.; Zhang, L.; Grenèche, J. M.; Hémon-Ribaud, A.; Leblanc, M.; Guiet, A.; Galven,
31 C.; Tarascon, J. M.; Maisonneuve, V.; Lhoste, J. New Amorphous Iron-Based Oxyfluorides as
32 Cathode Materials for High-Capacity Lithium-Ion Batteries. *J. Phys. Chem. C* **2019**, *123* (35),
33 21386–21394. <https://doi.org/10.1021/acs.jpcc.9b06055>.
- 34
35
36
37
38 (47) Li, N.; Keane, T. P.; Veroneau, S. S.; Nocera, D. G. Role of Electrolyte Composition on the Acid
39 Stability of Mixed-Metal Oxygen Evolution Catalysts. *Chem. Commun.* **2020**, *56* (72), 10477–
40 10480. <https://doi.org/10.1039/d0cc03863f>.
- 41
42
43
44
45 (48) Li, N.; Keane, T. P.; Veroneau, S. S.; Hadt, R. G.; Hayes, D.; Chen, L. X.; Nocera, D. G.
46 Template-Stabilized Oxidic Nickel Oxygen Evolution Catalysts. *Proc. Natl. Acad. Sci. U. S. A.*
47 **2020**, *117* (28), 16187–16192. <https://doi.org/10.1073/pnas.2001529117>.
- 48
49
50
51 (49) Kim, J. S.; Kim, B.; Kim, H.; Kang, K. Recent Progress on Multimetal Oxide Catalysts for the
52 Oxygen Evolution Reaction. *Advanced Energy Materials*. Wiley-VCH Verlag April 16, 2018.
53 <https://doi.org/10.1002/aenm.201702774>.
- 54
55
56
57
58
59
60

- 1
2
3 (50) Tao, H. B.; Xu, Y.; Huang, X.; Chen, J.; Pei, L.; Zhang, J.; Chen, J. G.; Liu, B. A General Method
4 to Probe Oxygen Evolution Intermediates at Operating Conditions. *Joule* **2019**, 3 (6), 1498–
5 1509. <https://doi.org/10.1016/j.joule.2019.03.012>.
6
7
8
9
10
11
12
13
14

15 TOC Image



1
2
3
4
5
6
7
8
9
10
11
12
13
14
15
16
17
18
19
20
21
22
23
24
25
26
27
28
29
30
31
32
33
34
35
36
37
38
39
40
41
42
43
44
45
46
47
48
49
50
51
52
53
54
55
56
57
58
59
60